

# Computational Studies of the Primary Phototransduction Event in Visual Rhodopsin

JOSÉ A. GASCÓN,  
EDUARDO M. SPROVIERO, AND  
VICTOR S. BATISTA\*

Department of Chemistry, Yale University, P. O. Box 208107,  
New Haven, Connecticut 06520-8107

Received September 7, 2005

## ABSTRACT

This Account addresses recent advances in the elucidation of the detailed molecular rearrangements due to the primary photochemical event in rhodopsin, a prototypical G-protein-coupled receptor (GPCR) responsible for the signal transmission cascade in the vertebrate vision process. The reviewed studies provide fundamental insight on long-standing problems regarding the assembly and function of the individual residues and bound water molecules that form the rhodopsin active site, a center that catalyzes the 11-cis/all-trans isomerization of the retinyl chromophore in the primary step of the phototransduction mechanism. Emphasis is placed on the authors' recent computational studies, based on state-of-the-art quantum mechanics/molecular mechanics (QM/MM) hybrid methods, addressing the structural refinement of the retinyl chromophore binding site in high-resolution X-ray structures of bovine visual rhodopsin, the energy storage mechanism, and the molecular origin of spectroscopic changes due to the primary photochemical event.

## 1. Introduction

Understanding the role played by highly conserved amino acid residues and bound water molecules in the activation of G-protein-coupled receptors (GPCRs) has been a subject of great interest for many years (see references in refs 1 and 2). GPCRs are macromolecules of great biological interest since they regulate transduction of events from the extracellular environment to the interior of every cell. The process of vision, for instance, starts with the activation of rhodopsin, a prototype of a vast subclass of GPCRs. After exposure to light, rhodopsin undergoes a series of

José A. Gascón received his B.Sc. degree in Physics from FAMAF, Argentina (1996), and his Ph.D. degree in Chemistry from Louisiana State University (2002). Since 2003, he has been working under the supervision of Prof. Batista at Yale University in QM/MM studies of biomacromolecules.

Eduardo M. Sproviero received his Lic. in Physics degree (1994) and his Ph.D. in Physics (2003) from UBA, Argentina. Since 2004, he has been a member of Prof. Batista's research group at Yale, working on QM/MM studies of inorganic, organic, and biological molecules.

Victor S. Batista received his Lic. Ciencias Químicas degree from UBA, Argentina (1989), and the Ph.D. degree in Chemistry from Boston University (1996). He completed postdoctoral programs with Prof. William H. Miller at the University of California, Berkeley (1997–1999), and with Prof. Paul Brumer at the University of Toronto (2000). He joined the Yale faculty in 2001, where he is currently Associate Professor of Chemistry. He has received the Sugata Ray Award (1995), the ACS PRF-G6 Award (2002), the Research Corporation Innovation Award (2002), the NSF Career Award (2004), the Sloan Fellowship (2005–2006), and the Camille Dreyfus Teacher–Scholar Award (2005).

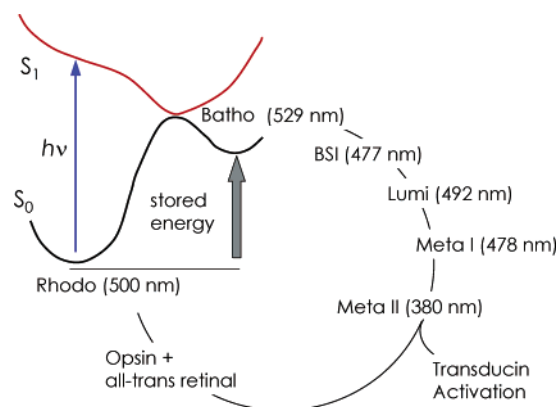


FIGURE 1. Schematic representation of the phototransduction cycle.

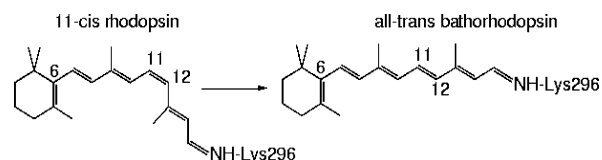


FIGURE 2. Photoisomerization of the retinyl chromophore in rhodopsin.

conformational changes leading to the binding of the G-protein transducin and later activation of GTP (Figure 1), triggering the visual transduction process.<sup>3,4</sup>

This Account reviews recent progress made by rigorous computational studies of visual rhodopsin, the sole member of the GPCR family whose crystal structure has been solved at high resolution. The studies are based on quantum-mechanics/molecular-mechanics (QM/MM) hybrid methods, which are currently state-of-the-art computational methodologies for studying challenging prosthetic groups embedded in biological molecules (e.g., the retinyl chromophore in visual rhodopsin).<sup>1,2</sup> The reviewed studies provide new insight concerning the detailed molecular rearrangements responsible for the primary activation event, the underlying energy storage mechanism and the assignment and characterization of NMR and photoabsorption spectroscopic changes due to the 11-cis/all-trans isomerization of the retinyl chromophore in visual rhodopsin, depicted in Figure 2.

The detailed molecular structure of the rhodopsin binding pocket has been the subject of prolonged investigations and remains an open problem.<sup>1,2,5–7</sup> Recent breakthroughs in X-ray crystallography<sup>5,8–10</sup> have made significant contributions toward a complete atomistic description of the protein structure. However, even with these important advances in X-ray crystallography, the resolution remains insufficient to unequivocally define the parts functionally important to the chromophore binding site.<sup>5</sup>

In the absence of an unequivocal X-ray definition of the chromophore-binding site, several structural and mechanistic aspects of the rhodopsin binding pocket remain poorly understood. These problems have been the

\* To whom correspondence should be addressed. E-mail: victor.batista@yale.edu.

subject of extensive work in NMR spectroscopy, as well as FTIR and resonance-Raman spectroscopic studies (see references in refs 1 and 2); however, the theoretical interpretation of this wealth of experimental data does not yet lead to a fully consistent molecular picture in terms of the spatial, electronic, and vibrational structure of the system.<sup>11</sup> In particular, contradictory aspects emerging from NMR experimental data include the double-bond character of C14–C15, the distribution of the net-positive charge along the extended  $\pi$ -system, the nature of non-bonding interactions between the retinylidene ionone ring and the protein, and the orientation of the  $\beta$ -ionone ring relative to the polyene chain. Furthermore, the characterization of molecular rearrangements due to the isomerization process, the energy storage mechanism, and the structural and functional roles of highly conserved amino acid residues remain uncertain.

Current theoretical work on the primary photochemical event in visual rhodopsin builds upon a long history of computational studies,<sup>12–15</sup> most of which were performed long before the X-ray structures of visual rhodopsin became available.<sup>5,8–10</sup> These early studies certainly provided valuable insight on the isomerization process; however, rigorous models of the influence of the protein environment were not possible since the protein structure was not known.

Breakthroughs in X-ray crystallography have already motivated theoretical studies, including calculations based on classical molecular dynamics simulations,<sup>16–18</sup> *ab initio* restricted Hartree–Fock (RHF) calculations of reduced-model systems,<sup>11,19</sup> and studies based on QM/MM hybrid methods.<sup>1,2,5–7,20–22</sup> In particular, recent DFT QM/MM studies<sup>1,2</sup> have addressed the elucidation of chromophore–opsin interactions responsible for phototransduction and energy storage through 11-cis/all-trans isomerization, a problem that has been largely elusive to first-principles examinations. Some of the fundamental questions are as follows: What are the molecular rearrangements responsible for 11-cis/all-trans isomerization in the rhodopsin binding pocket? What is the nature of the chromophore–protein interactions responsible for the torque that causes isomerization? Is there a preferential direction for the isomerization of the chromophore? How does the protein environment affect the primary reaction process? What is the role played by bound water molecules during the isomerization process? Is there a perturbational effect due to the extracellular loop II (EII)? How is the photon energy stored through 11-cis/all-trans isomerization? Is the stored energy mostly due to charge separation? Is the salt bridge between the protonated Schiff base (pSB) and the negative counterion Glu-113 stable upon photoisomerization? What is the orientation of the  $\beta$ -ionone ring relative to the polyene chain? How are the <sup>1</sup>H and <sup>13</sup>C NMR chemical shifts of the chromophore affected by the isomerization process? What is the nature of the interactions responsible for changes in chemical shifts? These questions are addressed herein by summarizing the main structural and mechanistic findings emerging from rigorous DFT QM/MM studies.<sup>1,2</sup> Due to lack of space, earlier computations

and contributions from other research groups are mentioned only briefly.

## 2. Isomerization Process

Rigorous DFT QM/MM computational methods have been applied to investigate the molecular rearrangements due to the primary photochemical event in rhodopsin.<sup>1</sup> These studies have applied a practical methodology based on two fundamental assumptions. First, it has been assumed that protein relaxation occurs only after the 11-cis/all-trans isomerization of the retinyl chromophore is completed. This assumption is consistent with the experimentally observed 200 fs reaction time,<sup>23,24</sup> as well as with the observation that the isomerization coordinate is mainly coupled to the vibrational modes of the retinyl chromophore.<sup>25</sup> Second, it has also been assumed that the molecular structure of the all-trans retinyl chromophore in the ground electronic state, produced by curve-crossing dynamics after photoexcitation of the system, relaxes to the same minimum energy configuration as that when the chromophore is isomerized along the ground-state minimum energy path (MEP).<sup>1</sup> These two assumptions have been partially validated by the favorable comparison between the predicted energy storage and calorimetry measurements (see section 3), as well as by the agreement between the experimental and predicted changes in NMR chemical shifts due to 11-cis/all-trans isomerization (see section 7). Furthermore, the implemented assumptions are consistent with the recent observation of thermal activation of visual pigments,<sup>26</sup> indicating that activation by light and by heat may in fact follow the same molecular route.

Computationally, these assumptions allow one to bypass the problem of solving the excited-state relaxation process. Relaxed molecular structures of bathorhodopsin can then be obtained by generating relaxed intermediate structures along the ground-state MEP, subject to the constraints of a fixed  $\phi$ (C11–C12) dihedral angle.<sup>1</sup> Optimized structures are thus obtained by geometry optimization at the ONIOM-EE (B3LYP/6-31G\*:Amber) level of theory after incrementally rotating  $\phi$ (C11–C12) in the 0° to –180° range. The geometry relaxation must include the retinyl chromophore, the bound water molecules, and all residues within a 20 Å radius from the chromophore. The protein structure beyond the 20 Å radius must be subject to harmonic constraints to preserve the natural shape of the protein.

Figure 3 shows the underlying conformational changes due to the 11-cis/all-trans isomerization in bovine visual rhodopsin. It is shown that the isomerization reaction changes the  $\phi$ (C11–C12) dihedral angle (highlighted in magenta) from –11° in the 11-cis isomer to –161° in the all-trans isomer. The preferential negative sense of rotation of the  $\phi$ (C11–C12) dihedral angle is determined by the steric van der Waals interactions between Ala-117 and the polyene chain at the C13 position. Note that the  $\beta$ -ionone ring, the Schiff base linkage (highlighted in blue), and the protein chain beyond the linkage (highlighted in

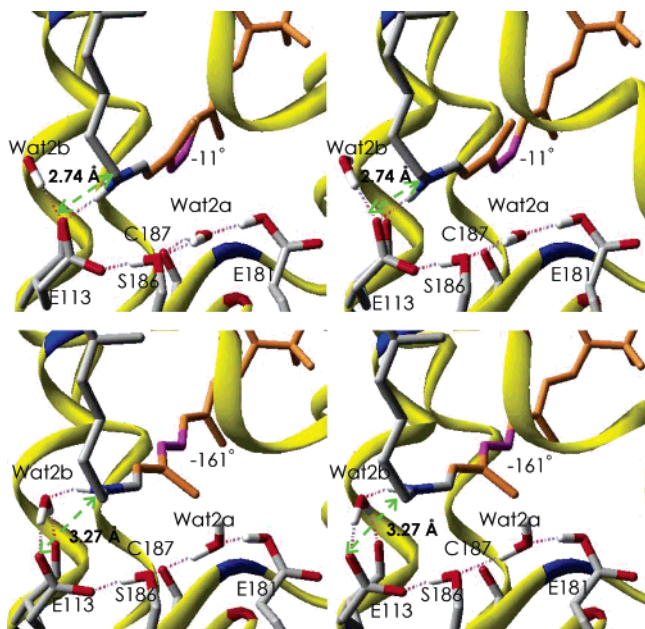


**FIGURE 3.** Molecular rearrangements due to the 11-cis/all-trans photoisomerization of the retinyl chromophore in visual rhodopsin (steric views).

gray) remain mostly undisplaced after isomerization of the retinyl chromophore. The constraints for molecular rearrangements in the rhodopsin binding pocket are due to the steric interactions at both ends of the retinyl chromophore, including motion restrictions due to interactions between the three methyl-substituent groups in the  $\beta$ -ionone ring and the surrounding residues, and the almost 90° turn of the protein backbone at the C- $\alpha$  atom of Lys-296 beyond the Schiff base linkage. These constraints fix both ends of the chromophore during the isomerization reactions, inducing torsional structural rearrangements in the polyene chain segment extending from C6 to the Schiff base linkage. Figure 4 shows the superposition of optimized molecular structures for the reactant 11-cis rhodopsin (brown) and the product all-trans bathorhodopsin (white). It is shown that the isomerization induces a reorientation of the C13-methyl substituent group and the consequent torsion of the polyene chain at the protonated NH(+) Schiff base linkage to Lys-296. The underlying torsion of the linkage induces a reorientation of polarized

bonds, including the C15–H and N–H<sup>+</sup> bonds with partial positive charges on the H atoms (see Figure 5 for a close-up view).

The analysis of electrostatic potential (ESP) atomic charges<sup>27</sup> indicates that the reorientation of the two polarized bonds N–H(+) and C15–H, during the isomerization process, accounts for the displacement of the net positive charge at the linkage relative to the negatively charged counterion Glu-113, even when the linkage itself remains almost undisplaced.

The comparative analysis of the chromophore dihedral angles in 11-cis rhodopsin and all-trans bathorhodopsin<sup>1</sup> indicates that the polyene chain is significantly bent and twisted in the all-trans form with out-of-the-plane distortions larger than 20° in the dihedral angles along the C9–C10, C12–C13, C14–C15, and C15–NH(+) chromophore bonds. These structural changes can be compared to the molecular rearrangements in the “bicycle-pedal” pathway proposed<sup>12</sup> and refined<sup>14</sup> by Warshel and co-workers before the rhodopsin crystal structure was available, where the 180° rotation around the C11–C12 bond is compensated by a 40° twist around the C9–C10 and C15–N bonds. As described earlier in this section, the ONIOM-EE (B3LYP/6-31G\*:Amber) level predicts that the isomerization reaction involves a 150° rotation around the C11–C12 bond compensated by distortions larger than 20° in the dihedral angles along the C9–C10, C12–C13, C14–C15, and C15–NH(+) bonds. Remarkably, the larger distortions predicted by the ONIOM-EE (B3LYP/6-31G\*:Amber) level correspond approximately to 30° twists around the C9–C10, C14–C15, and C15–N bonds, in partial agreement with the “bicycle-pedal” model. The torsion around the C15–N bond, however, is found to be crucial for the reorientation of polarized bonds leading to storage of electrostatic energy.

### 3. Energy Storage

The energy storage predicted at the ONIOM-EE (B3LYP/6-31G\*:Amber) level, as the energy difference between cis and trans isomers, is 34 kcal/mol<sup>1</sup> in excellent agreement with calorimetry measurements reported in the 32–35 kcal/mol energy range.<sup>28</sup> A correction factor of ~4 kcal/



**FIGURE 4.** Superposition of molecular structures of 11-cis rhodopsin (brown) and all-trans bathorhodopsin (white), optimized at the ONIOM-EE (B3LYP/6-31G\*:Amber) level of theory (steric views).

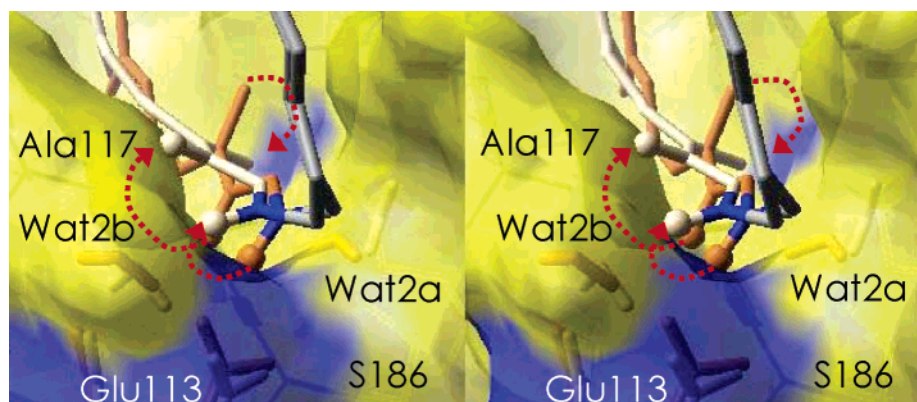


**FIGURE 5.** Superposition of rhodopsin (brown) and bathorhodopsin (white) molecular structures at the Schiff base linkage (steric views).

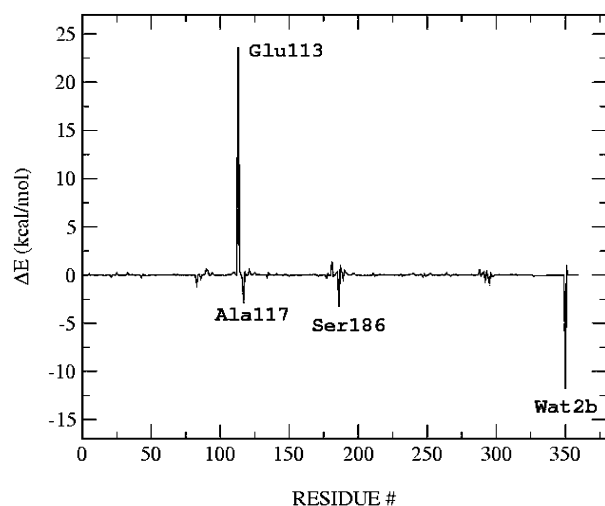


**FIGURE 6.** Electrostatic contribution of each residue to the total energy storage.

**Table 1. Energy Storage due to 11-Cis/All-Trans Isomerization in Rhodopsin as Predicted by the ONIOM-EE(B3LYP/6-31G\*:Amber) Theory**

total energy storage	34.1 kcal/mol
electrostatic contribution	17.1 kcal/mol (50%)
strain contribution	11.1 kcal/mol (32%)
van der Waals contribution	5.9 kcal/mol (18%)
experimental value	32.2 ± 0.9 kcal/mol <sup>29</sup>
	34.7 ± 2.2 kcal/mol <sup>28</sup>

mol, due to the influence of room-temperature thermal fluctuations, has been estimated by finite temperature free energy calculations (see Supporting Information). The decomposition of the total energy storage into electrostatic, strain, and van der Waals energy contributions is presented in Table 1. Such a decomposition shows that 50% of the energy storage is due to electrostatic interactions, 32% is due to strain energy, and the remaining 18% corresponds to van der Waals interactions.

To quantify the electrostatic contributions from individual amino acid residues, the endothermicity has been recomputed after zeroing the atomic charges of all residues except for the specific amino acid residue of interest. These calculations, reported in Figure 6, provide a systematic analysis over all residues and bound water molecules in the system. It is found that the most important electrostatic contributions result from interac-

tions between the retinyl chromophore and only a few highly conserved polar residues in the rhodopsin binding pocket, including Glu-113, Ser-186, and Ala-117 and Wat2b. These important residues are spatially distributed in the rhodopsin binding pocket as displayed in Figure 5. As expected, Figure 6 indicates that the largest electrostatic contribution to the total energy storage results from the negatively charged counterion Glu-113.

At this point, it is important to mention that the ONIOM-EE (B3LYP/6-31G\*:Amber) theory predicts almost identical ESP atomic charges for the pSB retinyl chromophore in 11-cis rhodopsin or all-trans bathorhodopsin. Therefore, only the reorientation of the polarized bonds C15–H and N–H<sup>+</sup> accounts for the displacement of the net positive charge relative to the negatively charged counterion Glu-113. Thus, the resulting charge separation mechanism is mainly based on rotation of the polarized bonds C15–H and N–H<sup>+</sup> with only a minor displacement of the C15–N linkage relative to the counterion Glu-113. The underlying molecular rearrangements responsible for storage of electrostatic energy are thus significantly different from previously postulated charge separation processes based upon displacement of the polyene chain linkage away from the carboxylate counterion toward a nonpolar environment.<sup>12–14,30</sup>

The molecular rearrangements due to the photoisomerization in visual rhodopsin have been recently analyzed at the QM/MM (CASPT2//CASSCF/6-31G\*:Amber) level<sup>6</sup> through partial geometry relaxation with respect to the configuration of the chromophore, Lys-296, and nearby water molecules. The bathorhodopsin product was found to be only partially isomerized with  $\phi(\text{C11}–\text{C12}) = -145^\circ$ , and the endothermicity was predicted to be only 26 kcal/mol, mainly due to strain energy within the chromophore. In contrast, DFT QM/MM studies<sup>1</sup> suggest that including complete relaxation of the surrounding protein environment confirms a thermodynamically stable isomerization product, more completely isomerized (e.g., with  $\phi(\text{C11}–\text{C12}) = -161^\circ$ ), with an overall endothermicity of 34 kcal/mol with only 11 kcal/mol of strain energy due to steric interactions with the protein environment.

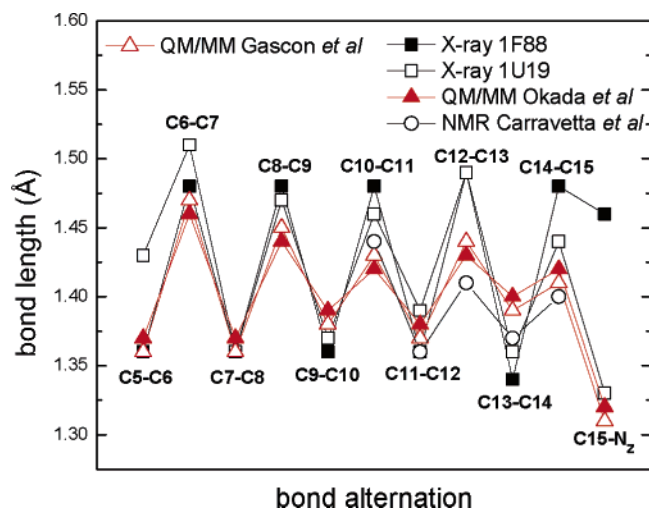


**FIGURE 7.** Bond-length alternation along the polyene chain of the 11-cis retinyl chromophore in rhodopsin, including the X-ray crystal structures 1F88, 1HZX, 1L9H, and 1U19, the QM/MM-MD (SCC-DFTB:CHARMM) structure,<sup>5</sup> a recent NMR structure,<sup>32</sup> and the QM/MM ONIOM-EE (B3LYP:AMBER) model.<sup>1</sup>

#### 4. Structural Analysis

Figure 7 compares bond lengths along the polyene chain of the chromophore in currently available X-ray, NMR, and QM/MM structures of visual rhodopsin in the 11-cis dark state. These results show that the QM/MM computational models are quite consistent with one another, both showing a much less pronounced alternation of C–C bond lengths along the polyene chain (see zigzag of red triangles, Figure 7) than in the X-ray structures (black squares, Figure 7). Furthermore, both QM/MM models predict a shorter N(Lys-296)–O(Glu-113) distance (not shown in Figure 7) when compared to the crystal structures. Further, the X-ray structures show significant dispersion in the reported values of bond lengths and C11–C12 dihedral angles. The latter ranges from  $-36^\circ$  in the 1U19 crystal structure,<sup>5</sup> to  $-1^\circ$  in 1F88,  $8^\circ$  in 1HZX, and  $0^\circ$  in 1L9H. In contrast, the ONIOM-EE and SCC-DFTB QM/MM models have a smaller dispersion and predict the C11–C12 dihedral angle to be  $-11^\circ$ <sup>1</sup> and  $-18^\circ \pm 9^\circ$ ,<sup>5</sup> respectively. Both of these QM/MM results are also in reasonable agreement with molecular dynamics simulations based on a force field where the parameters for the retinyl chromophore dihedral angles were adjusted according to the corresponding values of ab initio calculations.<sup>17</sup> As pointed out by Okada et al.,<sup>5</sup> the structural differences between X-ray and QM/MM models seem to result from difficulties faced by the X-ray refinement software when dealing with chemically unusual structures, such as the twisted and extended  $\pi$ -system and the carboxylate group interacting with the delocalized charge of the extended chromophore.

Comparisons between DFT and CASSCF calculations of reduced model systems, where only the retinyl chromophore has been relaxed, indicate that DFT methods might underestimate the underlying bond alternation pattern.<sup>7,31</sup> However, it is important to note that the weaker bond-length alternation predicted by DFT QM/

MM models of the complete system (i.e., with a fully relaxed retinyl chromophore and surrounding protein environment) is in very good agreement with a recent double-quantum solid-state NMR study<sup>32</sup> (see open circles in Figure 7). The reduction in bond-length alternation near the Schiff base linkage might be attributed to partial delocalization of the net positive charge in the pSB since such a delocalization of positive charge is expected to reduce the bond order of CC double bonds.

#### 5. Charge Distribution

The hypothesis that a reduction in bond-length alternation near the Schiff base linkage is due to delocalization of the net positive charge in the pSB has been originally suggested by NMR studies, where the partial double-bond character for the C14–C15 bond was attributed to penetration of a polaronic charge defect in the conjugated chain.<sup>33–35</sup> In contrast, however, resonance Raman data<sup>25,36,37</sup> and recent double-quantum solid-state NMR experiments<sup>32</sup> converge toward single-bond character for C14–C15, suggesting that the polaronic charge defect might hop over the vicinity of the Schiff base, settling in the middle of the polyene chain next to C12.<sup>32</sup> An objective of recent DFT QM/MM studies has been to resolve such a contradictory picture by providing a detailed first principles description of the electronic density of the chromophore as influenced by the protein environment.<sup>1,2</sup>

To analyze the extent of positive charge delocalization along the polyene chain, Figure 8 (upper panel) shows the distribution of electronic density difference after and before protonation of the retinyl chromophore in the rhodopsin binding site. It is shown that protonation of the Schiff base linkage induces electronic charge redistribution, driving electronic density from the polyene chain toward the NH<sup>+</sup> bond (see violet isosurface). As a consequence, a partial positive charge (green isosurface) is injected in the polyene chain according to an alternating pattern along the segment C9–C15.

The influence of nearby polar residues on the delocalization of positive charge has been analyzed by computing the electronic density difference due to protonation of the chromophore, after zeroing (i.e., switching-off) all atomic charges in the EII loop and Wat2a (see Figure 8, lower panel). The comparison between the upper and lower panels of Figure 8 shows that the electrostatic influence of EII and Wat2a accounts for small changes in the delocalization of positive charge along the polyene chain. However, it is noticeable that switching-off the electrostatic influence of EII and Wat2a enhances the alternating pattern of charge distribution, extending the delocalization of charge throughout the polyene chain (see, e.g., positive charge density at the C7 position). These results partially agree with a recent suggestion made by solid-state NMR studies,<sup>32</sup> where polar amino acid residues in the EII loop and Wat2a were thought to stabilize the positive charge near C12. The QM/MM results reported in Figure 8, however, do not support the assessment that the positive charge is being “pulled away” from the Schiff base

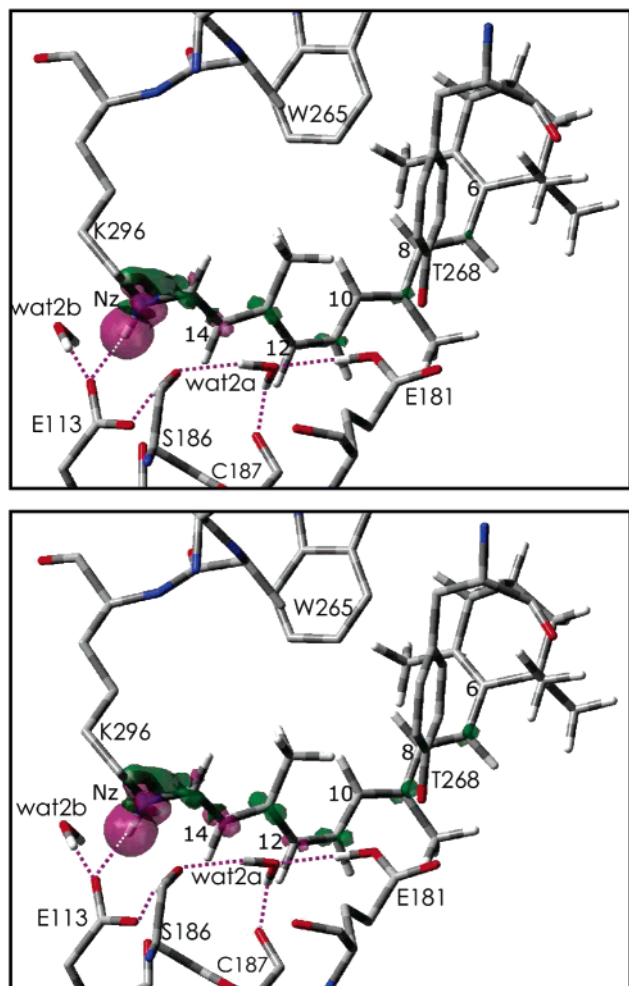


**FIGURE 8.** Iso-surface of electronic density difference, after and before protonation of the chromophore (upper panel) indicating the extent of delocalization of positive charge (green color) along the polyene chain and (lower panel) delocalization with atomic charges in the EII loop and Wat2a set to zero.

linkage.<sup>32</sup> Rather than pulling positive charge away from the linkage, the electrostatic influence of EII and Wat2a concentrates the positive charge next to the Schiff base linkage within the C9–C15 segment, a charge distribution that would otherwise be more delocalized along the entire  $\pi$ -system. Furthermore, the reoptimization of rhodopsin at the ONIOM-EE (B3LYP/6-31G\*:Amber) level after zeroing all atomic charges in the EII and Wat2a indicates that the absence of electrostatic interactions with EII and Wat2a does not significantly alter the bond-length alternation pattern along the polyene chain. In fact, a very similar alternation pattern is found in computational models of the chromophore in solution.<sup>2</sup>

## 6. Photoabsorption Spectra

QM/MM simulations of the photoabsorption spectroscopy of 11-cis visual rhodopsin and all-trans bathorhodopsin have been based on calculations of  $S_0 \rightarrow S_1$  vertical electronic-excitation energies.<sup>1</sup> Table 2 summarizes the computational results obtained at the ONIOM-EE (TD-B3LYP/6-31G\*:Amber) level of theory after optimization

**Table 2. Electronic-Excitation Energies (kcal/mol) for  $S_0 \rightarrow S_1$  Transitions in Rhodopsin, Bathorhodopsin, and Retinal in Methanol**

	$\Delta E_{\text{rhod}}$	$\Delta E_{\text{batho}}$	retinal (in methanol)
ONIOM-EE (TD-B3LYP/6-31G*:Amber)	59.4	59.0	66.8
QM/MM (CASPT2//CASSCF/6-31G*:Amber)	59.7 <sup>b</sup>	57.1	
experimental values	57.4 <sup>a</sup>	54.0 <sup>a</sup>	76.2 <sup>c</sup>

<sup>a</sup> Reference 38. <sup>b</sup> Reference 6. <sup>c</sup> Reference 39.

of molecular structures at the ONIOM-EE (B3LYP/6-31G\*:Amber) level.<sup>1</sup> These results are compared to both the corresponding experimental data and recent QM/MM (CASPT2//CASSCF/6-31G\*:Amber) calculations by Olivucci and co-workers.<sup>22</sup> For completeness, Table 2 also reports vertical excitation energies for the retinal chromophore in methanol,<sup>1</sup> computed in terms of an implicit solvent model at the B3LYP/6-31G\* level of theory. It is shown that the ONIOM-EE (TD-B3LYP//B3LYP/6-31G\*:Amber) level of theory predicts vertical excitation energies in very good agreement with both the QM/MM CASPT2 calculations and experimental values within a 3% and 9% error, respectively. However, the predicted opsin shift, defined as the vertical excitation energy shift for the chromophore in solution and inside the protein, is only in good qualitative agreement with experimental measurements, probably due to the simplifying approximation inherent in the implicit solvent model.

## 7. NMR Spectroscopy

The recently reported DFT QM/MM simulations of the NMR spectroscopy of the retinyl chromophore in visual rhodopsin<sup>2</sup> represent a rigorous attempt to model the chromophore <sup>1</sup>H NMR and <sup>13</sup>C NMR chemical shifts with an explicit treatment of the influence of the surrounding protein environment. The reported results show that the computational models of 11-cis rhodopsin and all-trans bathorhodopsin describe the chromophore NMR spectroscopy in very good agreement with solid-state NMR experiments, including not only the opsin effects on chemical shifts but also the underlying changes in chemical shifts due to the 11-cis/all-trans isomerization in the rhodopsin binding pocket. These DFT QM/MM simulations thus validate the computational models and provide rigorous first-principle interpretations of the rhodopsin NMR spectra.

**7.1. <sup>1</sup>H NMR.** The upper panel of Figure 9 compares the calculated <sup>1</sup>H NMR chemical shifts of the 11-cis retinyl chromophore in rhodopsin to the corresponding experimental data. The agreement between ab initio and experimental values indicates that the computational models are able to reproduce the <sup>1</sup>H NMR spectroscopy of the chromophore in both the rhodopsin and solution environments, including significant differences in chemical shifts between the more unshielded <sup>1</sup>H nuclei attached to sp<sup>2</sup> carbon atoms in the C7–C15 segment ( $\sigma^{\text{P}} = 6\text{--}7$  ppm range) and the more protected sp<sup>3</sup> carbon atoms ( $\sigma^{\text{C}}$

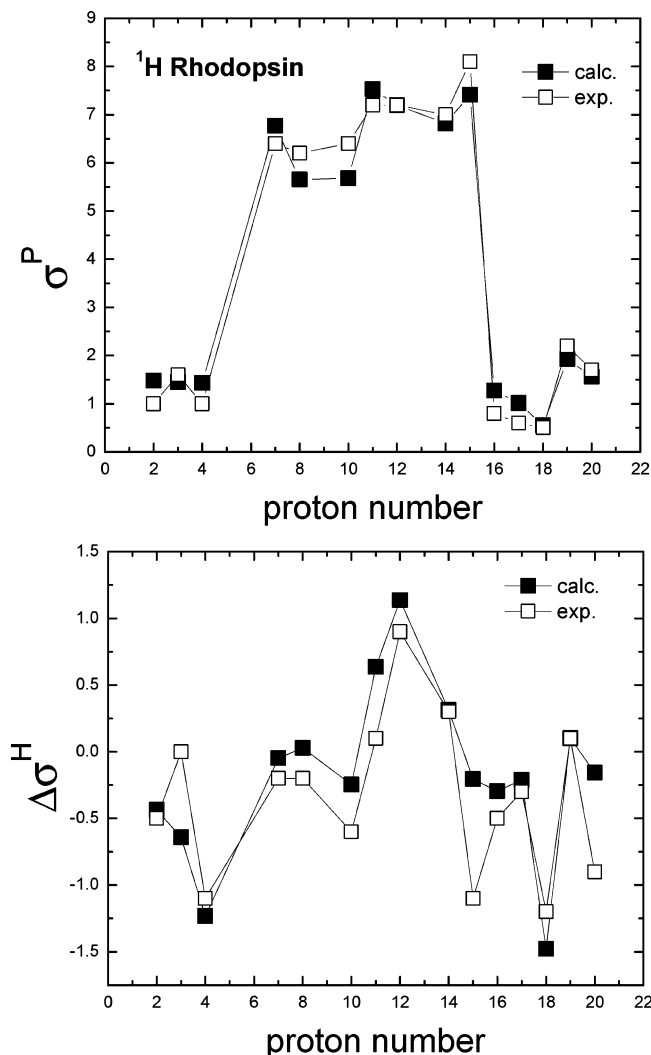


**FIGURE 9.** (upper panel)  $^1\text{H}$  NMR chemical shifts (in ppm) of the 11-cis retinyl chromophore in rhodopsin,  $\sigma_{\text{rhod}}^{\text{H}}$  and (lower panel) comparison of theoretical and experimental values of changes in the  $^1\text{H}$  NMR chemical shifts of the 11-cis retinyl chromophore (in ppm),  $\Delta\sigma^{\text{H}} = \sigma_{\text{rhod}}^{\text{H}} - \sigma_{\text{sol}}^{\text{H}}$ , due to the influence of the rhodopsin environment (i.e., the opsin effects on  $^1\text{H}$  NMR chemical shifts as described in the text).

= 0.3–2 ppm range) in the methyl-substituent groups and the  $\beta$ -ionone ring.

To compare the NMR spectroscopy of the retinyl chromophore embedded in the protein and the corresponding spectrum for the chromophore in solution,<sup>40</sup> computational models of the 11-cis retinyl–propylinium–chloride complex in chloroform solution were constructed by geometry optimization of the complex embedded in a polarizable continuum model (PCM) solvent ( $\epsilon_{\text{sol}} = 4.9$ ).<sup>2</sup> The lower panel of Figure 9 compares theoretical and experimental values of changes in the chromophore  $^1\text{H}$  NMR chemical shifts,  $\Delta\sigma^{\text{H}} = \sigma_{\text{rhod}}^{\text{H}} - \sigma_{\text{sol}}^{\text{H}}$ , due to the influence of the rhodopsin environment (i.e., the opsin effects on  $^1\text{H}$  NMR chemical shifts). In semiquantitative agreement with experimental data, the ab initio calculations at the DFT B3LYP/6-31G\* level of theory predict that the most significant influence of the protein environment is to unshield  $^1\text{H}$  nuclei in the C11–C14 segment, while

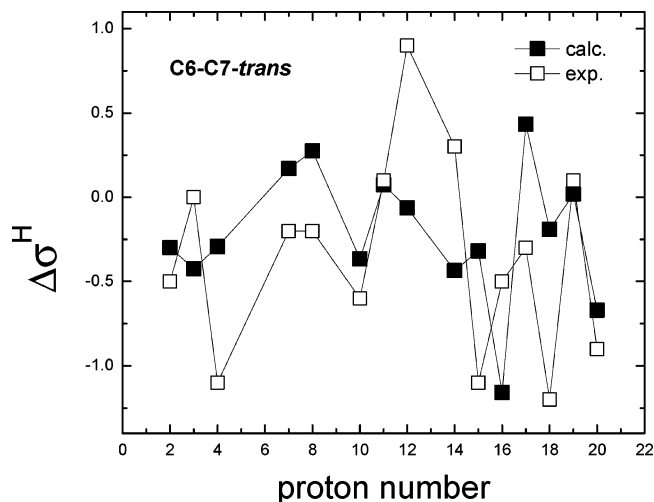


**FIGURE 10.** Changes in the  $^1\text{H}$  NMR chemical shifts of the 6s-trans retinyl chromophore,  $\Delta\sigma^{\text{H}} = \sigma_{\text{rhod}}^{\text{H}} - \sigma_{\text{sol}}^{\text{H}}$ , due to the influence of the rhodopsin environment.

nearby residues partially shield protons in the  $\beta$ -ionone ring, including H-4 and H-18. The theoretical predictions, however, underestimate changes in chemical shifts of H-15 and H-20 probably due to the oversimplified description provided by the reaction field of the PCM dielectric solvent.

**7.2. Orientation of the  $\beta$ -Ionone Ring.** The orientation of the  $\beta$ -ionone ring relative to the polyene chain has been the subject of debate<sup>33,41–44</sup> and is defined by the configuration about the C6–C7 single bond of the retinyl chromophore. In particular, NMR studies by Watts and co-workers,<sup>41</sup> as well as theoretical work by Birge and co-workers,<sup>42</sup> concluded that the chromophore geometry is 6s-trans at the C6–C7 bond, in contrast to the 6s-cis conformation assumed by earlier NMR and optical studies.<sup>33,43,45–50</sup>

To address the orientation of the  $\beta$ -ionone ring, according to rigorous DFT QM/MM calculations, a computational model of the 6s-trans isomer has been constructed by geometry relaxation of the system after rotation of the  $\beta$ -ionone ring around the C6–C7 bond.<sup>2</sup> The resulting 6s-trans structure, obtained at the ONIOM electronic-embedding (B3LYP/6-31G\*:Amber) level of theory, was found to be as stable as the 6s-cis isomer for many thermally accessible configurations and about 8 kcal/mol less stable than the 6s-cis structure when minimum energy geometries are compared. Consistently, the  $^1\text{H}$  NMR spectrum of the 6s-trans isomer compares much less favorably to experimental data than the spectrum of the 6s-cis isomer (see Figure 10 and lower panel of Figure 9).

Figure 10 presents the comparison between the opsin effects on the  $^1\text{H}$  NMR chemical shifts of the 6s-trans chromophore ( $\Delta\sigma^{\text{H}} = \sigma_{\text{rhod}}^{\text{H}} - \sigma_{\text{sol}}^{\text{H}}$ ) and the corresponding experimental data, indicating that the 6s-trans isomer compares less favorably to experimental data than the 6s-cis isomer. It is, therefore, concluded that although both structures are of comparable stability, the orientation of the  $\beta$ -ionone ring relative to the polyene chain must be locked in the 6s-cis configuration. Such a 6s-cis structure

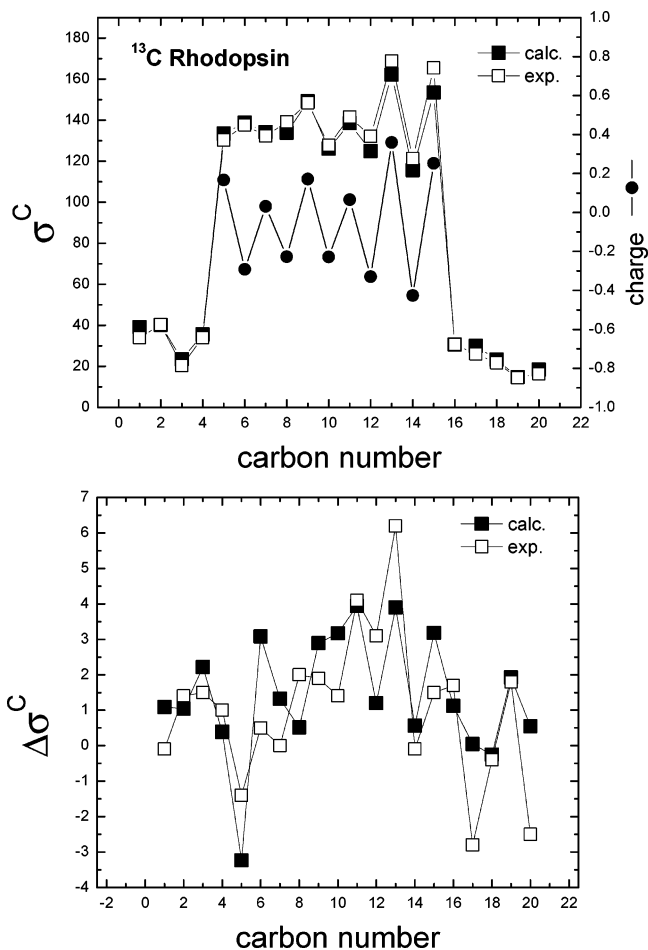


**FIGURE 11.** (upper panel)  $^{13}\text{C}$  NMR chemical shifts (in ppm) of the 11-cis retinyl chromophore in rhodopsin,  $\sigma_{\text{rhod}}^{\text{C}}$ , and ESP atomic charges of carbon atoms with  $\text{sp}^2$  hybridization reported in solid circles and (lower panel) comparison of theoretical and experimental values of changes in the  $^{13}\text{C}$  NMR chemical shifts of the 11-cis retinyl chromophore (in ppm),  $\Delta\sigma^{\text{H}} = \sigma_{\text{rhod}}^{\text{C}} - \sigma_{\text{sol}}^{\text{C}}$ , due to the influence of the rhodopsin environment.

is characterized by a substantial negative twist of the dihedral angle ( $-44^\circ$ ) at the C6–C7 bond.<sup>1</sup> These theoretical results are partially consistent with recent NMR studies<sup>43,44</sup> and with the analysis of the recently resolved X-ray structure at 2.2 Å resolution.<sup>5</sup>

**7.3.  $^{13}\text{C}$  NMR.** Upper panel of Figure 11 compares theoretical and experimental values of  $^{13}\text{C}$  NMR chemical shifts associated with the 11-cis retinyl chromophore in rhodopsin. These results indicate that the computational models are able to reproduce the  $^{13}\text{C}$  NMR spectroscopy of the chromophore in both rhodopsin and solution environments, including the description of significant differences in chemical shifts between the unshielded carbon atoms with  $\text{sp}^2$  hybridization in the C7–C15 segment ( $\sigma^{\text{C}} = 115\text{--}160$  ppm range) and the more protected  $\text{sp}^3$  carbon atoms ( $\sigma^{\text{C}} = 20\text{--}40$  ppm range). The alternating pattern of chemical shifts in the C7–C15 segment is found to be partially correlated with the corresponding alternation of atomic charges along the polyene chain (see solid circles in Figure 11).

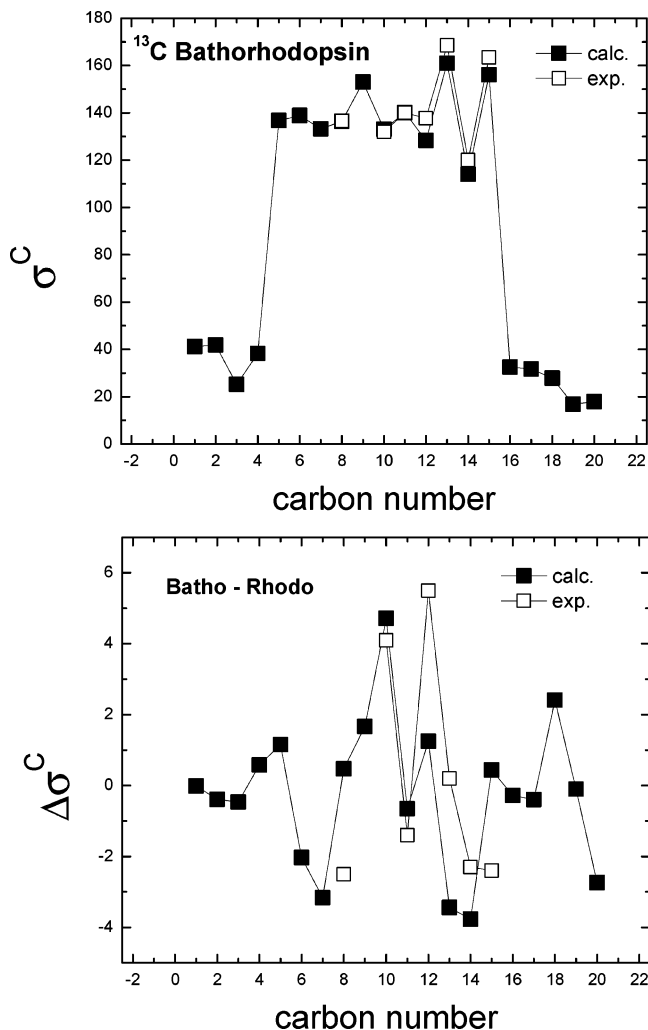


**FIGURE 12.** Comparison of  $^{13}\text{C}$  NMR chemical shifts (in ppm) of the all-trans retinyl chromophore in bathorhodopsin,  $\sigma_{\text{rhod}}^{\text{C}}$  (upper panel), and the difference between  $^{13}\text{C}$  NMR chemical shifts in bathorhodopsin and rhodopsin (lower panel).

The lower panel of Figure 11 compares theoretical and experimental values of changes in the chromophore  $^{13}\text{C}$  NMR chemical shifts,  $\Delta\sigma^{\text{C}} = \sigma_{\text{rhod}}^{\text{C}} - \sigma_{\text{sol}}^{\text{C}}$ , due to the influence of the rhodopsin environment (i.e., the opsin effects on  $^{13}\text{C}$  NMR chemical shifts).<sup>2</sup> In agreement with experimental data, these simulations predict that the protein environment unshields all  $^{13}\text{C}$  nuclei except C5 in the retinyl chromophore. The overall agreement between theoretical and experimental data is quite satisfactory, specially considering that  $^{13}\text{C}$  NMR chemical shifts are often reported with errors as large as  $\pm 1$  ppm and larger when different studies are compared.<sup>33,43</sup> The theoretical predictions, however, seem to underestimate changes in chemical shifts of C17 and C20, due to an overestimation of the chemical shifts of the corresponding methyl-substituent groups in rhodopsin.

An important aspect addressed by recent DFT QM/MM simulations<sup>2</sup> is the observed upfield shift of  $\sigma^{\text{C}}$  at C5, which has been previously assigned to the interaction between C5 and the carboxylic group of Glu-122.<sup>43</sup> However, QM/MM calculations indicate that the electrostatic influence of Glu-122 is negligible when such a residue is protonated

as suggested by FTIR experiments.<sup>49</sup> In contrast, QM/MM studies found that the most significant upfield shift on C5 is due to Trp-265, with an upfield effect of  $-2.0$  ppm.<sup>2</sup> This upfield effect, however, is almost completely canceled by the  $1.8$  ppm downfield shift due to Asp-190. Therefore, it is concluded that the net upfield shift of  $\sigma^C$  at C5 is not determined by the nearby residue with the largest upfield contribution but rather by the overall polarization of the  $\pi$ -system, predominantly modulated by the counterion Glu-113. However, mutations of either Trp-265 or Asp-190 should produce a significant effect on the  $^{13}\text{C}$  NMR spectrum at the C5 position.

Figure 12 (upper panel) compares the calculated  $^{13}\text{C}$  NMR chemical shifts of the all-trans retinyl chromophore in bathorhodopsin to readily available experimental data, including  $^{13}\text{C}$  NMR chemical shifts for C8, C10, C11, C12, C13, C14, and C15.<sup>50</sup> In addition, Figure 12 (lower panel) presents theoretical and experimental values of changes in the chromophore  $^{13}\text{C}$  NMR chemical shifts,  $\Delta\sigma^C = \sigma_{\text{batho}}^C - \sigma_{\text{rhod}}^C$ , due to the 11-cis/all-trans isomerization. The comparison presented in Figure 12 shows good qualitative agreement between theoretical and readily available experimental data, partially supporting the underlying molecular rearrangements elucidated through DFT QM/MM refinement of high-resolution X-ray structures.<sup>1</sup>

## 8. Concluding Remarks

This Account outlines recent advances in the emergence of rigorous DFT QM/MM studies of molecular rearrangements and spectroscopic changes associated with the primary phototransduction event in visual rhodopsin. The reviewed computational work addresses fundamental questions that, for many years, have remained largely elusive to rigorous first-principles examinations. The reviewed studies reveal that state-of-the-art DFT QM/MM hybrid methods constitute powerful tools of modern computational chemistry when applied in conjunction with high-resolution crystal structures. These methods are thus expected to make many more important contributions in studies of GPCRs as well as in the general field of chemical reactivity in biological molecules.

V.S.B. acknowledges supercomputer time from NERSC and financial support from Research Corporation Grant No. RI0702, the American Chemical Society PRF No. 37789-G6, the NSF Career Program CHE No. 0345984, the NSF ECS Grant No. 0404191, the Alfred P. Sloan Fellowship (2005–2006), a Camille Dreyfus Teacher-Scholar Award for 2005, and a Yale Junior Faculty Fellowship in the Natural Sciences (2005–2006).

**Supporting Information Available:** Descriptions of the structural models, the QM/MM method, and the finite temperature calculations. This material is available free of charge via the Internet at <http://pubs.acs.org>.

## References

- Gascón, J. A.; Batista, V. S. QM/MM Study of Energy Storage and Molecular Rearrangements due to the Primary Event in Vision. *Biophys. J.* **2004**, *87*, 2931–2941.
- Gascón, J. A.; Sproviero, E. M.; Batista, V. S. QM/MM Study of the NMR Spectroscopy of the Retinyl Chromophore in Visual Rhodopsin. *J. Chem. Theory Comput.* **2005**, *1*, 674–685.
- Nikiforovich, G. V.; Marshall, G. R. Three-Dimensional Model for M-II Rhodopsin, an Activated G-Protein-Coupled Receptor. *Biochemistry* **2003**, *42*, 9110–9120.
- Baylor, D. How photons start vision. *Proc. Natl. Acad. Sci. U.S.A.* **1996**, *93*, 560–565.
- Okada, T.; Sugihara, M.; Bondar, A.; Elstner, M.; Entel, P.; Buss, V. The Retinal Conformation and its Environment in Rhodopsin in Light of a New  $2.2 \text{ \AA}$  Crystal Structure. *J. Mol. Biol.* **2004**, *342*, 571–583.
- Andrúniów, T.; Ferre, N.; Olivucci, M. Structure, initial excited-state relaxation, and energy storage of rhodopsin resolved at the multiconfigurational perturbation theory level. *Proc. Natl. Acad. Sci. U.S.A.* **2004**, *101*, 17908–17913.
- Blomgren, F.; Larsson, S. Exploring the Potential Energy Surface of Retinal, a Comparison of the Performance of Different Methods. *J. Comput. Chem.* **2005**, *26*, 738–742.
- Palczewski, K.; Kumasaka, T.; Hori, T.; Behnke, C. A.; Motoshima, H.; Fox, B. A.; Le Trong, I.; Teller, D. C.; Okada, T.; Stenkamp, R. E.; Yamamoto, M.; Miyano, M. Crystal structure of rhodopsin: A G protein-coupled receptor. *Science* **2000**, *289*, 739–745.
- Teller, D.; Okada, T.; Behnke, C.; Palczewski, K.; Stenkamp, R. Advances in determination of a high-resolution three-dimensional structure of rhodopsin, a model of G-protein-coupled receptors (GPCRs). *Biochemistry* **2001**, *40*, 7761–7772.
- Okada, T.; Yoshinori, Y.; Silow, M.; Navarro, J.; Landau, J.; Schichida, Y. Functional role of internal water molecules in rhodopsin revealed by X-ray crystallography. *Proc. Natl. Acad. Sci. U.S.A.* **2002**, *99*, 5982–5987.
- Touw, S.; de Groot, H. J. M.; Buda, F. Ab Initio Modeling of the Spatial, Electronic, and Vibrational Structure of Schiff Base Models for Visual Photoreceptors. *J. Phys. Chem. B* **2004**, *108*, 13560–13572.
- Warshel, A. Bicycle-pedal model for 1st step in vision process. *Nature* **1976**, *260*, 679–683.
- Weiss, R. M.; Warshel, A. A New View of the Dynamics of Singlet cis–trans Photoisomerization. *J. Am. Chem. Soc.* **1979**, *101*, 6131–6133.
- Warshel, A.; Barboy, N. Energy-storage and reaction pathways in the first step of the vision process. *J. Am. Chem. Soc.* **1982**, *104*, 1469–1476.
- Birge, R.; Cooper, T. Energy-storage in the primary step of the photocycle of bacteriorhodopsin. *Biophys. J.* **1983**, *42*, 61–69.
- Rohrig, U. F.; Guidoni, L.; Rothlisberger, U. Early steps of the intramolecular signal transduction in rhodopsin explored by molecular dynamics simulations. *Biochemistry* **2002**, *41*, 10799–10809.
- Saam, J.; Tajkhorshid, E.; Hayashi, S.; Schulten, K. Molecular Dynamics investigation of the primary photoinduced events in the activation of rhodopsin. *Biophys. J.* **2002**, *83*, 3097–3112.
- Furutani, Y.; Shichida, Y.; Kandori, H. Structural changes of water molecules during the photoactivation processes in bovine rhodopsin. *Biochemistry* **2003**, *42*, 9619–9625.
- Yamada, A.; Kakitani, T.; Yamamoto, S.; Yamato, T. A computational study on the stability of the protonated Schiff base of retinal in rhodopsin. *Chem. Phys. Lett.* **2002**, *366*, 670–675.
- Sugihara, M.; Buss, V.; Entel, P.; Elstner, M.; Frauenheim, T. 11-cis-Retinal protonated Schiff base: Influence of the protein environment on the geometry of the rhodopsin chromophore. *Biochemistry* **2002**, *41*, 15259–15266.
- Sugihara, M.; Entel, P.; Buss, V. A first-principles study of 11-cis-retinal: Modelling the chromophore-protein interaction in rhodopsin. *Phase Transitions* **2002**, *75*, 11–17.
- Ferre, N.; Olivucci, M. Probing the rhodopsin cavity with reduced retinal models at the CASPT2/CASSCF/AMBER level of theory. *J. Am. Chem. Soc.* **2003**, *125*, 6868–6869.
- Schoenlein, R.; Peteanu, L.; Mathies, R.; Shank, C. The first step in vision – femtosecond isomerization of rhodopsin. *Science* **1991**, *254*, 412–415.
- Wang, Q.; Schoenlein, R. W.; Peteanu, L. A.; Mathies, R. A.; Shank, C. V. Vibrationally coherent photochemistry in the femtosecond primary event of vision. *Science* **1994**, *266*, 422–424.
- Palings, I.; Pardo, J.; den Berg, E. V.; Winkel, C.; Lugtenburg, J.; Mathies, R. A. Assignment of fingerprint vibrations in the resonance Raman-spectra of rhodopsin, isorhodopsin and bathorhodopsin- Implications for chromophore structure and environment. *Biochemistry* **1987**, *26*, 2544–2556.
- Ala-Laurila, P.; Donner, K.; Koskelainen, A. Thermal activation and photoactivation of visual pigments. *Biophys. J.* **2004**, *86*, 3653–3662.

- (27) Gascón, J. A.; Leung, S. S. F.; Batista, E. R.; Batista, V. S. A Self-Consistent Space-Domain Decomposition Method for QM/MM Computations of Protein Electrostatic Potentials. *J. Chem. Theor. Comput.* **2006**, *2*, 175–186.
- (28) Cooper, A. Energy uptake in the 1st step of visual excitation. *Nature* **1979**, *282*, 531–533.
- (29) Schick, G.; Cooper, T.; Holloway, R.; Murray, L.; Birge, R. Energy-storage in the primary photochemical events of rhodopsin and isorhodopsin. *Biochemistry* **1987**, *26*, 2556–2562.
- (30) Honig, B.; Ebrey, T. G.; Callender, R. H.; Dinur, U.; Callender, R. H. Photoisomerization, energy-storage, and charge separation – model for light energy transduction in visual pigments and bacteriorhodopsin. *Proc. Natl. Acad. Sci. U.S.A.* **1979**, *76*, 2503–2507.
- (31) Page, C.; Olivucci, M. Ground and excited-state CASPT2 geometry optimizations of small organic molecules. *J. Comput. Chem.* **2003**, *24*, 298–309.
- (32) Carravetta, M.; Zhao, X.; Johannessen, O. G.; Lai, W. C.; Verhoeven, M. A.; Bovee-Geurts, P. H. M.; Verdegem, P. J. E.; Kiihne, S.; Luthman, H.; de Groot, H. J. M.; de-Grip, W. J.; Lugtenburg, J.; Levitt, M. H. Protein-Induced Bonding Perturbation of the Rhodopsin Chromophore Detected by Double-Quantum Solid-State NMR. *J. Am. Chem. Soc.* **2004**, *126*, 3948–3953.
- (33) Smith, S. O.; Palings, I.; Miley, M. E.; Courtin, J.; de Groot, H.; Lugtenburg, J.; Mathies, R. A.; Griffin, R. G. Solid-State NMR Studies of the Mechanism of the Opsin Shift in the Visual Pigment Rhodopsin. *Biochemistry* **1990**, *29*, 8158–8164.
- (34) Verdegem, P. J. E.; Bovee-Geurts, P. H. M.; de Grip, W. J.; Lugtenburg, J.; de Groot, H. J. M. Retinylidene Ligand Structure in Bovine Rhodopsin, Metarhodopsin-I, and 10–19 Methylrhodopsin from Internuclear Distance Measurements Using <sup>13</sup>C-Labeling and 1-D Rotational Resonance MAS NMR. *Biochemistry* **1999**, *38*, 11316–11324.
- (35) Feng, X.; Verdegem, P. J. E.; Lee, Y. K.; Sandström, D.; Edén, M.; Bovee-Geurts, P. H. M.; de Grip, W. J.; Lugtenburg, J.; Levitt, M. H. Direct Determination of a Molecular Torsional Angle in the Membrane Protein Rhodopsin by Solid-State NMR. *J. Am. Chem. Soc.* **1997**, *119*, 6853–6857.
- (36) Eyring, G.; Curry, B.; Broek, A.; Lugtenburg, J.; Mathies, R. A. Assignment and interpretation of hydrogen out-of-plane vibrations in the resonance Raman-spectra of rhodopsin and bathorhodopsin. *Biochemistry* **1982**, *21*, 384–394.
- (37) Lin, S. W.; Groesbeek, M.; van der Hoef, I.; Verdegem, P.; Lugtenburg, J.; Mathies, R. A. Vibrational assignment of torsional normal modes of rhodopsin: Probing excited-state isomerization dynamics along the reactive C11=C12 torsion coordinate. *J. Phys. Chem. B* **1998**, *102*, 2787–2806.
- (38) Pan, D.; Mathies, R. A. Chromophore structure in lumirhodopsin and metarhodopsin I by time-resolved resonance Raman microchip spectroscopy. *Biochemistry* **2001**, *40*, 7929–7936.
- (39) Anarboldi, M.; Motto, M. G.; Tsujimoto, K.; Balogh-Nair, V.; Nakanishi, K. Hydroretinals and Hydrorhodopsins. *J. Am. Chem. Soc.* **1979**, *101*, 7082–7084.
- (40) Shriver, J. W.; Mateescu, G. D.; Abrahamson, E. W. Proton and C-13 nuclear magneticresonance spectroscopy study of the conformation of a protonated 11-cis-retinal schiff-base. *Biochemistry* **1979**, *18*, 4785–4792.
- (41) Gröbner, G.; Burnett, I. J.; Glaubitz, C.; Choi, G.; Mason, A. J.; Watts, A. Observations of light-induced structural changes of retinal within rhodopsin. *Nature* **2000**, *405*, 810–813.
- (42) Birge, R. Conformation and orientation of the retinyl chromophore in rhodopsin: A critical evaluation of recent NMR data on the basis of theoretical calculations results in a minimum energy structure consistent with all experimental data. *Biochemistry* **2001**, *40*, 4201–4204.
- (43) Creemers, A. F. L.; Kiihne, S.; Bovee-Geurts, P. H. M.; DeGrip, W. J.; Lugtenburg, J.; de Groot, H. J. M. <sup>1</sup>H and <sup>13</sup>C MAS NMR evidence for pronounced ligand-protein interactions involving the ionone ring of the retinylidene chromophore in rhodopsin. *Proc. Natl. Acad. Sci. U.S.A.* **2002**, *99*, 9101–9106.
- (44) Spooner, P. J. R.; Sharples, J. M.; Goodall, S. C.; Seedorf, H.; Verhoeven, M. A.; Lugtenburg, J.; Bovee-Geurts, P. H. M.; DeGrip, W. J.; Watts, A. Conformational similarities in the beta-ionone ring region of the rhodopsin chromophore in its ground state and after photoactivation to the metarhodopsin-I intermediate. *Biochemistry* **2003**, *42*, 13371–13378.
- (45) Smith, S. O.; Palings, I.; Copie, V.; Raleigh, D.; Courtin, J.; Pardoën, J.; Lugtenburg, J.; Mathies, R.; Griffin, R. G. Low-temperature solid-state <sup>13</sup>C NMR studies of the retinal chromophore in rhodopsin. *Biochemistry* **1987**, *26*, 1606–1611.
- (46) Tan, Q.; Lou, J.; Borhan, B.; Karnaukhova, E.; Berova, N.; Nakanishi, K. Absolute sense of twist of the C12–C13 bond of the retinal chromophore in bovine rhodopsin based on excitoncoupled CD spectra of 11,12-dihydroretinal analogues. *Angew. Chem., Int. Ed. Engl.* **1997**, *36*, 2089–2093.
- (47) Jäger, S.; Lewis, J.; Zvyaga, T.; Szundi, I.; Sakmar, T.; Kliger, D. Chromophore Structural Changes in Rhodopsin from Nanoseconds to Microseconds following pigment photolysis. *Proc. Natl. Acad. Sci. U.S.A.* **1997**, *94*, 8557–8562.
- (48) Buss, V.; Kolster, K.; Terstegen, F.; Vahrenhorst, R. Absolute sense of twist of the C12–C13 bond of the retinal chromophore in rhodopsin-semiempirical and nonempirical calculations of chiroptical data. *Angew. Chem., Int. Ed.* **1998**, *37*, 1893–1895.
- (49) Fahmy, K.; Jäger, F.; Beck, M.; Zvyaga, T. A.; Sakmar, T. P.; Siebert, F. Protonation states of membrane-embedded carboxylic acid groups in rhodopsin and metarhodopsin II – A Fourier-transform infrared-Spectroscopy study of site-directed mutants. *Proc. Natl. Acad. Sci. U.S.A.* **1993**, *90*, 10206–10210.
- (50) Smith, S. O.; Courtin, J.; de Groot, H.; Gebhard, R.; Lugtenburg, J. <sup>13</sup>C Magic-Angle Spinning NMR Studies of Bathorhodopsin, the Primary Photoproduct of Rhodopsin. *Biochemistry* **1991**, *30*, 7409–7415.

AR050027T